Acta metall. mater. Vol. 40, No. 9, pp. 2155–2165, 1992
Printed in Great Britain

0956-7151/92 $5.00 + 0.00
Pergamon Press Ltd

THEORY OF BONDING CHARGE DENSITY IN β' NiAl

Z. W. LU, S.-H. WEI and A. ZUNGER
National Renewable Energy Laboratory, Golden, CO 80401, U.S.A.

(Received 7 October 1991; in revised form 7 February 1992)

Abstract—Fox and Tabbernor [*Acta metall. mater.* **39,** 669 (1991)] have recently measured the four lowest structure factors $F(\mathbf{G})$ of NiAl using highly accurate high energy electron diffraction. We present here a systematic comparison of their results with *ab initio* band theory, in the context of the local density formalism. We find very good agreement for the three of the four lowest measured structure factors, while our $F(200)$ is ~ 0.4 e/cell higher. We tentatively attribute this difference to uncertainties in the treatment of the temperature factors in non-monoatomic compounds. Indeed, comparing with experiment our calculation for the monoatomic Si crystal (where the temperature term factors out), we find that theory reproduces the measured structure factors to within a very small deviations of ~ 0.02 e/atom. We have also examined the effect of high Fourier components that are not currently amenable to measurements on the ensuing NiAl deformation electron density distribution (DEDD) maps. We find that the truncation of the Fourier series after four structure factors misses the directional *d*-like charge lobes near the Ni sites. We show that static and dynamic DEDD give a similar picture of the bonding.

Résumé—Fox et Tabbernor [*Acta metall. mater.* **39,** 669 (1991)] ont récemment mesuré les quatre facteurs de structure ($F(\mathbf{G})$) les plus faibles de NiAl en utilisant la diffraction à haute précision d'électrons de haute énergie. Nous présentons ici une comparaison systématique de leurs résultats avec une théorie des bandes *ab initio*, dans le contexte du formalisme de la densité locale. Nous trouvons un très bon accord pour trois des quatre facteurs de structure, tandis que notre valeur de $F(200)$ est d'environ 0,4 e/maille plus élevée. Nous avons essayé d'attribuer cette différence à des incertitudes dans le traitement des facteurs de température dans les composés polyatomiques. En fait, quand nous comparons à l'expérience les calculs effectués pour le silicium cristallin monoatomique, dans lesquels le terme du facteur de température n'intervient pas, nous trouvons que la théorie reproduit les facteurs de structure mesurés avec une très bonne précision (environ 0,02 e/atome). Nous avons également examiné l'effet de composantes de Fourier élevées, qui ne sont généralement pas faciles à mesurer, sur les cartes de la distribution de la densité électronique de déformation (DDED) de NiAl. La troncature des séries de Fourier après quatre facteurs de structure ne rend pas compte des lobes directionnels de charges du type *d* près des sites de Ni. Nous montrons que les DDED statique et dynamique donnent une image similaire de la liaison.

Zusammenfassung—Fox und Tabbernor [*Acta metall. mater.* **39,** 669 (1991)] haben vor kurzem die vier kleinsten Strukturfaktoren $F(\mathbf{G})$ von NiAl mit hochgenauer Beugung hochenergetischer Elektronen gemessen. Wir legen hier einen systematischen Vergleich dieser Ergebnisse mit *ab initio*-Bandstruktur-Rechnungen im Rahmen der lokalen-Dichte-Formulierung vort. Mit drei der vier Strukturfaktoren ergibt sich sehr gute Übereinstimmung; unsert Wert für $F(200)$ ist allerdings $\sim 0{,}4$ e/Zelle größer. Wir schreiben diese Differenz versuchsweise Unsicherheiten in der Behandlung der Temperaturfaktoren in nicht-monoatomaren Substanzen zu. Vergleichen wir unsere Berechnungen für monoatomares Silizium (bei dem die Temperaturfaktoren sich herausheben) mit dem Experiment, dann zeigt sich nämlich, daß die Theorie die gemessenen Strukturfaktoren bis auf kleinste Abweichungen von $\sim 0{,}02$ e/Zelle beschreibt. Außerdem wird der Einfluß hoher Fourierkomponenten untersucht, die augenblicklich Messungen auf den Karten der Verformung der Elektronendichteverteilung von NiAl (DEDD) nicht zugänglich sind. Wir finden, daß das Abbrechen der Fourierserie nach vier Strukturfaktoren die gerichteten *d*-artigen Verteilungen in der Nähe der Ni-Plätze verfehlt. Wir zeigen, daß statische und dynamische DEDDS ein ähnliches Bild der Bindung entwerfen.

1. INTRODUCTION

The recent development of X-ray Pendellösung [1, 2], high energy electron diffraction [3, 4], Gamma ray diffraction [5, 6], and accurate X-ray diffraction [7] techniques enable now measurements of low-angle crystalline structure factors with an unprecedented accuracy approaching in some cases [8] 0.1%. Recent applications to compounds, including the CsCl-type NiAl intermetallic [9] and the zinc blende semiconductor GaAs [10] produced, for the first time, a detailed picture of the charge density deformation maps in these systems. At the same time, these results [10] raised interesting questions [11] on the sufficiency of the first few (low-angle) structure factors in capturing the global charge redistribution upon the formation of the solid from spherical atoms. In this work we compare the charge density in NiAl as extracted from the recent critical voltage electron diffraction measurements of Fox and Tabbernor [9]

with the results of the self-consistent *ab initio* calculations based on the local density formalism [12, 13]. We focus on the following questions:

(i) How well can *ab initio* band theory describe the first few (low-angle) structure factors amenable to such experiments?
(ii) Can higher-index structure factors (that are difficult to measure by electron diffraction [9]) be neglected for the purpose of assessing the overall charge redistribution in the solid relative to free atoms?
(iii) Is the overall charge redistribution affected by the inclusion of the Debye–Waller temperature factors (that are difficult to calculate by *ab initio* methods)?
(iv) Can the charge redistribution in NiAl be characterized as predominantly "ionic", "covalent" or "metallic"?

Questions (i)–(iii) were addressed previously [10, 11] for GaAs in the context of the electron diffraction measurements of Zuo *et al.* We extend here our previous study to an intermetallic system.

2. CALCULATED AND MEASURED QUANTITIES

2.1. Total charge densities

We start by a summary of the measured (expt) [equations (1)–(5)] and calculated (calc.) [equations (6)–(8)] quantities that will be compared below.

Using the "rigid atom approximation" [14], the *dynamic* structure factors for momentum $\mathbf{G} = 2\pi/a$ (h, k, l) are

$$F_{\text{expt}}(\mathbf{G}) = \sum_{\alpha=1}^{M} \rho_\alpha(\mathbf{G}) e^{i\mathbf{G}\cdot\boldsymbol{\tau}_\alpha} \mathbf{T}_\alpha(\mathbf{G}) \tag{1}$$

where $\rho_\alpha(\mathbf{G})$ is the Gth Fourier component of the charge density contributed by sublattice α (whose position vector is $\boldsymbol{\tau}_\alpha$) in the unit cell, and $T_\alpha(\mathbf{G})$ is the α's site temperature coefficient

$$T_\alpha(\mathbf{G}) = e^{-\mathbf{G}\cdot\boldsymbol{\beta}_\alpha\cdot\mathbf{G}} \tag{2}$$

where $\boldsymbol{\beta}_\alpha$ is the anisotropic temperature coefficient tensor at site α, often approximated by the Debye–Waller factor $B_\alpha/16\pi^2$. Note that in this universally used approximation the existence of vibrational degrees of freedom is represented by the partitioning of the continuous three-dimensional charge density into sub-regions associated with identifiable atomic scattering centers α. The *dynamic* real-space charge density can be synthesized from the Fourier components (1) by summing them up to a maximum momentum $\mathbf{G}_{\max}$ available from diffraction experiments. This gives

$$F_{\text{expt}}(\mathbf{r}, G_{\max}) = \sum_{\mathbf{G}}^{G_{\max}} F_{\text{expt}}(\mathbf{G}) e^{i\mathbf{G}\cdot\mathbf{r}} \tag{3}$$

where the result naturally depends on the highest momentum ($G_{\max}$) included in this sum (as we will see below, current high-precision experiments are limited to rather small cut-off values $\mathbf{G}_{\max}$). If the temperature factor can be deconvoluted from equation (1), one can construct the *static* (purely electronic) structure factor

$$\rho_{\text{expt}}(\mathbf{G}) = \sum_{\alpha=1}^{M} \rho_\alpha(\mathbf{G}) e^{i\mathbf{G}\cdot\boldsymbol{\tau}_\alpha} \tag{4}$$

from which one can synthesize, in analogy with (3), the *static* electronic density

$$\rho_{\text{expt}}(\mathbf{r}, G_{\max}) = \sum_{\mathbf{G}}^{G_{\max}} \rho_{\text{expt}}(\mathbf{G}) e^{i\mathbf{G}\cdot\mathbf{r}} \tag{5}$$

(Note that we consistently denote dynamic and static quantities as F and ρ, respectively.)

While diffraction experiments produce discrete Fourier components of the charge density, electronic structure calculations for periodic crystals can produce the total static density $\rho_{\text{calc}}(\mathbf{r})$ directly in coordinate space. This is obtained by summing the wavefunctions squares over all occupied band indices i and Brillouin zone wavevectors $\mathbf{k}$ enclosed within the Fermi energy ϵ_F

$$\rho_{\text{calc}}(\mathbf{r}) = \sum_{i,\mathbf{k}}^{\epsilon_F} N_i(\mathbf{k}) \psi_i^*(\mathbf{k}, \mathbf{r}) \psi_i(\mathbf{k}, \mathbf{r}) \tag{6}$$

where $N_i(\mathbf{k})$ is the occupation numbers of band i. The Fourier components of the static density can then be computed yielding

$$\rho_{\text{calc}}(\mathbf{G}) = \frac{1}{\Omega} \int \rho_{\text{calc}}(\mathbf{r}) e^{-i\mathbf{G}\cdot\mathbf{r}}\, d\mathbf{r} \tag{7}$$

where Ω is the unit cell volume. Since only limited $\mathbf{G}$ values are accessible experimentally, to compare with experiment we then synthesize a truncated static density by filtering out all Fourier components above a given momentum of $G_{\max}$

$$\rho_{\text{calc}}(\mathbf{r}, G_{\max}) = \sum_{G}^{G_{\max}} \rho_{\text{calc}}(\mathbf{G}) e^{i\mathbf{G}\cdot\mathbf{r}}. \tag{8}$$

If the temperature factors can be deconvoluted from the measured structure factors, the resulting static density $\rho_{\text{expt}}(\mathbf{r}, G_{\max})$ of equation (5) can be compared with the calculated quantity $\rho_{\text{calc}}(\mathbf{r}, G_{\max})$ of equation (8). This was accomplished, for example for the monoatomic Si crystal [15]. Failing to do so requires the introduction of temperature factors into the calculated charge density. The obvious difficulty here is that while the *measured* structure factors represented by the "rigid atom approximation" [14] [equation (1)] naturally represent linear contributions from atomiclike scattering centers α, there is no *unique* way of partitioning the *calculated* three-dimensional density $\rho_{\text{calc}}(\mathbf{r})$ into atomiclike quantities. Consequently, even if the temperature coefficients $\{T_\alpha\}$ are known, it is not obvious how to associate them with identifiable "scattering centers" α in the calculated density for systems having more than one

α (compounds). A common simplication [16] is to define some sort of atom-averaged temperature factor $\langle T(\mathbf{G})\rangle$ that multiplies $\rho(\mathbf{G})$. While this procedure seems reasonable for compounds whose constituent bonded atoms have similar vibrational properties (hence, similar Debye–Waller factors), it is not obvious how accurate it is otherwise. Given that any partitioning of $\rho_{\text{calc}}(\mathbf{r})$ into atomiclike quantities is arbitrary, we will choose a physically appealing (but non-unique) scheme: having calculated a unique and continuous density $\rho_{\text{calc}}(\mathbf{r})$, we divide space into (i) "muffin-tin" (MT) spheres around each atom α and (ii) the remaining, interstitial volume between them. Denoting as $\rho_\alpha^{\text{MT}}(\mathbf{G})$ the Fourier transform of the charge density in the α's muffin-tin sphere (minus the tails of the interstitial density extrapolate into these spheres) and by $\rho_{\text{I}}(\mathbf{G})$ the Fourier transform of the interstitial (I) charge density (extended over whole space), we have the calculated *dynamic* structure factor

$$F_{\text{calc}}(\mathbf{G}) = \rho_{\text{I}}(\mathbf{G})e^{-\langle B\rangle G^2/16\pi^2} + \sum_{\alpha=1}^{M} \rho_\alpha^{\text{MT}}(\mathbf{G})e^{-B_\alpha G^2/16\pi^2} \quad (9)$$

where B_α are the measured Debye–Waller factors and $\langle B\rangle$ is their atomic average. Here $\rho_\alpha^{\text{MT}}(\mathbf{G})$ is calculated by taking an integral over $0 \leqslant r \leqslant R_{\text{MT}}$ while $\rho_{\text{I}}(\mathbf{G})$ is calculated as an integral over all space. (These forms assure that only smooth functions are Fourier transformed, thus avoiding numerical high-frequency noise.) The corresponding calculated dynamic charge density is then

$$F_{\text{calc}}(\mathbf{r}, G_{\max}) = \sum_{\mathbf{G}}^{G_{\max}} F_{\text{calc}}(\mathbf{G})e^{i\mathbf{G}\cdot\mathbf{r}} \quad (10)$$

which can be compared with $F_{\text{expt}}(\mathbf{r}, G_{\max})$ of equation (3).

2.2. Deformation electron density distribution

As has been recognized many times previously (e.g. see Ref. [9]), the Fourier series of the *total* density of equations (3), (5) and (8) converges very slowly since the sharp features of $\rho(\mathbf{r})$ associated with the rapid variation of the wavefunctions near the core give rise to many short-wavelength Fourier components. To overcome this difficulty one is then attempting to Fourier transform the *difference* between $\rho(\mathbf{r})$ and some model density $\rho_{\text{model}}(\mathbf{r})$ chosen such that the high Fourier components of the latter will approximately match those of $\rho(\mathbf{r})$. One is then focusing on the static *deformation* density distribution

$$\Delta\rho(\mathbf{r}) = \rho(\mathbf{r}) - \rho_{\text{model}}(\mathbf{r}) \quad (11)$$

or on its Fourier truncated form

$$\Delta\rho(\mathbf{r}, G_{\max}) = \sum_{\mathbf{G}}^{G_{\max}} [\rho(\mathbf{G}) - \rho_{\text{model}}(\mathbf{G})]e^{i\mathbf{G}\cdot\mathbf{r}}. \quad (12)$$

The dynamic counterpart of equation (12) is then $\Delta F(\mathbf{r}, G_{\max})$. The choices of ρ_{model} is obviously nonunique; a standard choice is to represent it as a superposition (sup) of spherically-symmetric neutral atomic ground state charge densities $n_\alpha(r)$, yielding the static result

$$\rho_{\text{sup}}(\mathbf{G}) = \sum_{\alpha=1}^{M} n_\alpha(\mathbf{G})e^{i\mathbf{G}\cdot\tau_\alpha} \quad (13)$$

and the dynamic result

$$F_{\text{sup}}(\mathbf{G}) = \sum_{\alpha=1}^{M} n_\alpha(\mathbf{G})e^{i\mathbf{G}\cdot\tau_\alpha}T_\alpha(\mathbf{G}) \quad (14)$$

where $n_\alpha(\mathbf{G})$ is the **G**th Fourier component of the free *atom* density $n_\alpha(r)$ [not to be confused with the *crystalline* quantity $\rho_\alpha(\mathbf{G})$ of equation (1)]. A variety of choices exist for $n_\alpha(r)$, e.g. Hartree–Fock results [9, 17], local density data [18], configuration-interaction, etc. The corresponding deformation electron density distribution (DEDD) is

$$\Delta\rho_{\text{sup}}(\mathbf{r}, G_{\max}) = \sum_{\mathbf{G}}^{G_{\max}} [\rho(\mathbf{G}) - \rho_{\text{sup}}(\mathbf{G})]e^{i\mathbf{G}\cdot\mathbf{r}}. \quad (15)$$

Including the temperature factors then yields

$$\Delta F_{\text{sup}}(\mathbf{r}, G_{\max}) = \sum_{\mathbf{G}}^{G_{\max}} [F(\mathbf{G}) - F_{\text{sup}}(\mathbf{G})]e^{i\mathbf{G}\cdot\mathbf{r}}. \quad (16)$$

An alternative choice [19] for the model density $\rho_{\text{model}}(\mathbf{r})$ is the charge density of the *solid* elemental constituents. For example, Fox and Tabbernor [9] interpolated the measured structure factors of solid f.c.c. Al and Ni, comparing them to those of NiAl. This procedure is complicated by the fact that the solid elemental constituents (Al and Ni) have the f.c.c. structure while NiAl is a b.c.c. subgroup. Furthermore, the molar volumes Ω of the constituents and the compound are very different. In what follows we will calculate the charge densities of Ni and Al in the hypothetical b.c.c. structure at the molar volume of NiAl. We will discuss the density deformation taken with respect to a superposition of free atoms [equation (15)] as well as that obtained with respect to the hypothetical b.c.c. elemental solids

$$\rho_{\text{model}}(\mathbf{r}) = \rho_{\text{b.c.c.}}(\mathbf{r}). \quad (17)$$

2.3. Purposes of the present study

The definitions introduced in Section 2.1 and 2.2 permit a clear statement of the issues we address in this paper [alluded to in the introduction, see items (i)–(iv) there]:

(i) How well do the dynamic structure factors $F_{\text{calc}}(\mathbf{G})$ [equation (9)] calculated from *ab initio* band theory reproduce the measured quantities $F_{\text{expt}}(\mathbf{G})$ of equation (1)?

(ii) Given that Fox and Tabbernor were able to measure only the lowest four structure factors of NiAl [i.e. up to $G_{\max} = 2\pi/a(2, 0, 0)$], one wonders whether the corresponding truncated deformation electron density distribution map $\Delta\rho_{\text{sup}}(\mathbf{r}, G_{\max})$ [equation (12)] suffices to capture the general features obtained with a higher cut-off momentum.

This question will be addressed by contrasting the *calculated* $\Delta\rho_{sup}(\mathbf{r}, G_{max})$ for increasing values of G_{max}. Note that in the case of GaAs, the five available [10] experimental structure factors, (111), (200), (220), (400) and (333) were previously shown [11] to be insufficient to capture the important details of $\Delta\rho_{sup}(\mathbf{r})$.

(iii) It has previously been suggested [20] that even when the high-index Fourier components of the *static* deformation density $[\rho(\mathbf{G}) - \rho_{sup}(\mathbf{G})]$ of equations (11) and (12) are non negligible, the temperature factors $e^{-BG^2/16\pi^2}$ will damp them. Consequently, the *dynamic* difference $[F(\mathbf{G}) - F_{sup}(\mathbf{G})]$ of equation (16) may be negligible for high G's, hence they can safely omitted from the DEDD. To test this practice, we will compare the dynamic $\Delta F_{sup}(\mathbf{r}, G_{max})$ with the static $\Delta\rho_{sup}(\mathbf{r}, G_{max})$ density deformation maps.

(iv) It has been previously shown [9] that in NiAl the momenta $\mathbf{G} = 2\pi/a(1, 0, 0)$ and $\mathbf{G} = 2\pi/a(1, 1, 1)$ contribute to the deformation density $\Delta F_{sup}(\mathbf{r})$ of equations (15) and (16) an "ionic" component (depletion of electron density near the Al site and accumulation on the Ni site), while the momentum component $\mathbf{G} = 2\pi/a(2, 0, 0)$ contributes a "covalent" charge (depletion of electron density from both the Al and Ni sites, and accumulation of density on the Ni–Al bond). One then wonders whether the *total* deformation density $\Delta\rho_{sup}(\mathbf{r})$ or $\Delta F_{sup}(\mathbf{r})$ (rather than specific $\mathbf{G}$ components) can be characterized as "ionic" or "covalent".

In addition to the issues, we will investigate whether alternative definitions of model density $\rho_{model}(\mathbf{r})$ of equation (11) [e.g. using for it the density of solid elemental constituents, equation (17)] leads to different conclusions concerning charge redistribution.

3. DETAILS OF CALCULATION

The single-particle wavefunctions $\psi(\mathbf{k}, \mathbf{r})$ of equation (6) are obtained by self-consistently solving the effective Schrödinger equation for a periodic NiAl solid in the CsCl structure

$$\{-\tfrac{1}{2}\nabla^2 + V_{e\text{-ion}}(\mathbf{r}) + V_{e\text{-e,C}} + V_{e\text{-e,X}} + V_{e\text{-e,CR}}\}\psi_i(\mathbf{k}, \mathbf{r}) = \epsilon_i(\mathbf{k})\psi_i(\mathbf{k}, \mathbf{r}) \quad (18)$$

where $V_{e\text{-ion}}$ is the electron–ion coulomb attraction, $V_{e\text{-e,C}}$ is the interelectronic (mean-field) Coulomb repulsion, $V_{e\text{-e,X}}$ is the average exchange interaction, $V_{e\text{-e,CR}}$ is the average correlation interaction and $\epsilon_i(\mathbf{k})$ are the band energies of band i at momentum $\mathbf{k}$. We use the local density description [12, 13] of $V_{e\text{-e,X}}$ and $V_{e\text{-e,CR}}$. The same conceptual framework was recently used to calculate electronic, magnetic and cohesive properties [21] of NiAl, energies of anti-phase boundaries in this material [22], its optical [23] and the photoemission properties [24], as well as thermodynamic and structural properties [25]. In this study we use the correlation functional $V_{e\text{-e,CR}}$ of Ceperley and Alder [26], as parameterized by Perdew and Zunger [27]. Equation (18) was solved self-consistently by the linearized augmented plane wave (LAPW) method [28], in which: (i) core and valence electrons are included simultaneously (i.e no pseudopotential approximation is used), (ii) no "shape approximations" to the potential or charge density are invoked (we expand the density and potential inside the muffin-tin spheres by lattice harmonics up to angular momentum of $l = 12$, while the interstitial region is described by a plane wave expansion with kinetic energy cutoff of 61.2 Ry), (iii) the electron–electron interactions are treated relativistically (using mass–velocity and Darwin terms [28]), except for spin-orbit effects which are neglected, and (iv) a large basis set consisting of both real-space orbitals (inside the muffin-tin regions) and plane waves is used. The total number of basis functions is ~ 110 per unit cell of 2 atoms. This basis set was found [25] to be sufficient to obtain structural energies to within 10 meV/atom, and to describe accurately the temperature–composition phase diagram of NiAl. We find that increasing the basis set to ~ 500 orbitals per unit cell and increasing the kinetic energy cut-off of the interstitial plane wave representation up to 148.2 Ry changes the Fourier components $\rho(100)$, $\rho(110)$, $\rho(111)$ and $\rho(200)$ by less than 0.1%. Our main approximation here is hence the use of the *local* density description of exchange and correlation [13].

We have used the room-temperature cubic lattice constant $a = 2.8864$ Å of β' NiAl [29]. The Brillouin zone sums of equation (6) were performed using 20 $\mathbf{k}$-vectors in the 1/48 irreducible section of the Brillouin zone. Extending this to 120 $\mathbf{k}$-vectors changes $\rho(200)$ by less than 0.1%. To calculate the dynamic structure factors in equation (9) we use the Debye–Waller factors $B_{Al} = 0.470$ and $B_{Ni} = 0.510$ of Georgopoulos and Cohen [30], used also by Fox and Tabbernor [9]. The muffin-tin radii used in this study were $R_{Al} = R_{Ni} = 1.2171$ Å; the fraction of the unit cell volume spanned by the spheres is 62.8%.

The atomic charge densities $n_\alpha(r)$ for $\alpha =$ Al, Ni were calculated from an equation analogous to equation (18) but with free-atom, rather than periodic boundary conditions and a spin-unrestricted Hamiltonian (since the atoms are "open-shell"). This Schrödinger equation was integrated numerically with high precision, so no basis functions were needed. In calculating the atomic densities n_α of equation (13) we used the ground state configurations $[Ne]2s^22p^1$ for Al and $[Ar]3d^8\,4s^2$ for Ni.

4. RESULTS

4.1. General features of the calculated static electron density

We first illustrate the need to cancel the high Fourier components of $\rho(\mathbf{r})$ to obtain a meaningful Fourier representation. The solid line in Fig. 1(a)

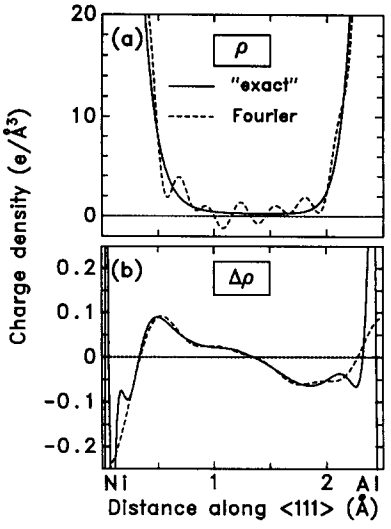

Fig. 1. (a) Static *total* electron density $\rho(\mathbf{r})$ along the nearest neighbor $\langle 111 \rangle$ direction. Solid line is the direct LAPW result [equation (6)] while the dashed line is the finite Fourier representation of the total electron density $\rho_{\text{calc}}(\mathbf{r}, G_{\text{big}})$ [equation (8)] using a very large cut-off $G_{\text{big}} = 2\pi/a(7, 6, 5)$, i.e. 163 stars. Clearly, even when that many stars are included in a Fourier series, it still exhibits significant oscillations in the bonding region missing in the "exact" density. (b) Analogous results for the static density deformation $\Delta\rho_{\text{sup}}(\mathbf{r})$ [from equation (15)], showing that this quantity is adequately described by a Fourier representation outside the core regions [even though we used a smaller cut-off $G_{\text{big}} = 2\pi/a(6, 3, 1)$].

gives the directly calculated ($G_{\max} \to \infty$) total electron density $\rho_{\text{calc}}(\mathbf{r})$ of equation (6). It is compared with the quantity $\rho_{\text{calc}}(\mathbf{r}, G_{\text{big}})$ of equation (8) (dashed line in Fig. 1) in which a very large cut-off $G_{\text{big}} = 2\pi/a(7, 6, 5)$ [equivalent to a total of 163 stars or 4944 individual plane waves, excluding the (0, 0, 0) star] was used. Clearly, even when as many as the first 163 stars of **G** are included in a Fourier representation the *total* density ρ [Fig. 1(a)] still exhibits significant oscillations in the bonding region. On the other hand, the density *difference* $\Delta\rho_{\text{sup}}(\mathbf{r}, G_{\text{big}})$ (equation (12) and Fig. 1(b)] obtained from a Fourier series using $G_{\text{big}} = 2\pi/a(6, 3, 1)$ closely mimics the directly calculated $\Delta\rho_{\text{sup}}(\mathbf{r})$ in the bonding regions [of course, $\Delta\rho_{\text{sup}}(\mathbf{r}, G_{\text{big}})$ still fails to reproduce the nodal structure near the core]. Note that the maximum magnitude of the static *deformation* density $\Delta\rho_{\text{sup}}(\mathbf{r})$ outside the core is only $\sim 0.1\ \text{e/Å}^3$, while the *total* density $\rho(\mathbf{r})$ has a magnitude of $\sim 10\ \text{e/Å}^3$ at this point. Clearly, the bonding charge is tiny.

Figure 2 shows as solid line the calculated static density *deformation* $\Delta\rho_{\text{sup}}(\mathbf{r})$ calculated without any Fourier truncation, comparing it to $\Delta\rho_{\text{sup}}(\mathbf{r}, G_{\text{big}})$ of equation (12), in which a large but finite cut-off $G_{\text{big}} = 2\pi/a(6, 3, 1)$ (54 stars) was used. We see again that while the Fourier representation rounds off the nodal structure in the core region, it does capture accurately the structure *outside* the core (~ 0.2 Å away from the center of Al and Ni) in all bonding directions. Figure 3 gives the same information as Fig. 2 but as a contour plot in the (110) plane: the untruncated density deformation $\Delta\rho_{\text{sup}}(\mathbf{r})$ [Fig. 3(a)] is seen to be similar to its Fourier representation $\Delta\rho_{\text{sup}}(\mathbf{r}, G_{\text{big}})$ in Fig. 3(b). Our deformation density is similar to the somewhat *noisier* previous calculation by Fu and Yoo [22(b)].

It is interesting to observe the general features of the calculated static density deformation $\Delta\rho_{\text{sup}}(\mathbf{r})$: if one ignores the core regions defined above (which we will discuss below), one finds an *accumulation* of density on the Ni sites with *depletion* on the Al sites [Fig. 1(b) and Fig. 2]. The density deformation on the *nearest* neighbor bond [Fig. 1(b)] shows a node near the center of the bond, while that on the *next* nearest neighbors (Fig. 2) is flat. Figure 3 shows as shaded regions the *directional* character of

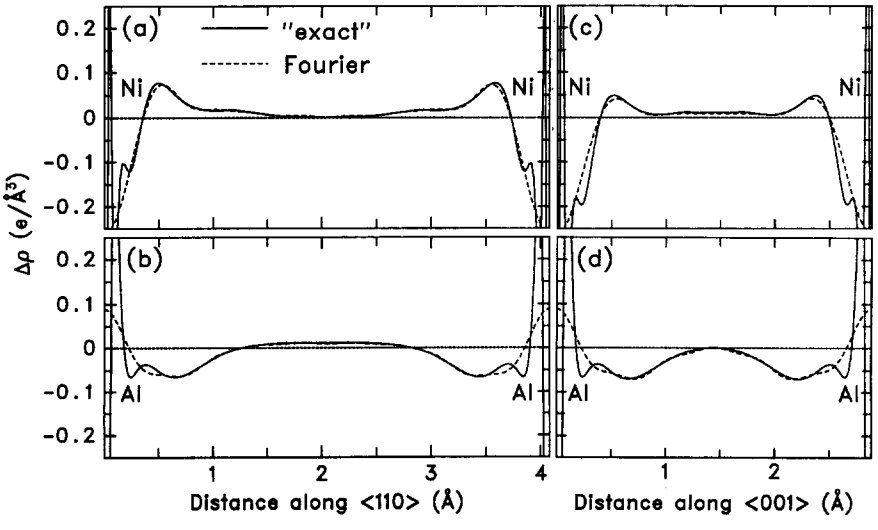

Fig. 2. Line plots of the static deformation density $\Delta\rho_{\text{sup}}(\mathbf{r}, G_{\text{big}})$ [equation (15)]. Solid line show the results without Fourier truncation ($G_{\max} \to \infty$), while dashed lines show the results of a Fourier synthesis with $G_{\text{big}} = 2\pi/a(6, 3, 1)$ or 54 stars.

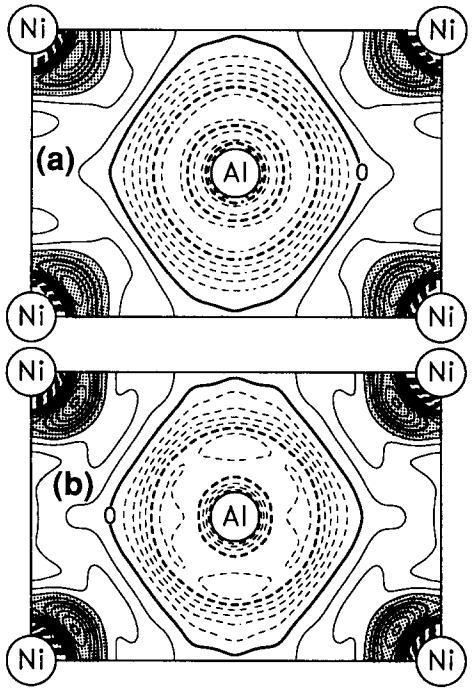

Fig. 3. Contour plots of the static deformation density $\Delta\rho_{sup}(\mathbf{r}, G_{big})$ [equation (15)]. (a) Without Fourier truncation; (b) with Fourier truncation at $G_{big} = 2\pi/a(6, 3, 1)$. Solid (dashed) lines represent positive (negative) values of $\Delta\rho$. The thick solid lines next to a dashed line gives the $\Delta\rho = 0$ contour. Contour spacing is 0.01 e/Å^3. The shaded areas denote the directional covalent charge accumulation near Ni pointing towards the Al sites.

the charge accumulation near Ni, discussed further below.

4.2. Comparison of experimental and calculated dynamic structure factors

Table 1 shows a rather good agreement (within ~ 0.6% or 80 me/cell) between the calculated $F_{calc}(\mathbf{G})$ and measured $F_{expt}(\mathbf{G})$ dynamic structure factors for the lowest three (100), (110) and (111) **G** values, while for the (200) beam the calculated value is 1.7% or ~ 400 me/cell *larger* than the measured value. Similar discrepancies were recently noted for GaAs [10].

A number of reasons could contribute to this discrepancy:

(1) Uncertainties in the Debye–Waller factors used in our calculations [equation (9)].
(2) Systematic theoretical errors in the *static* density.
(3) Systematic errors in the data analysis, including anharmonic factors, anomalous dispersion and the underlying association of the temperature factors $T_\alpha(\mathbf{G})$ with particular scattering sites [the "rigid atom approximation" of equation (1)].

To investigate (1) above we examine the sensitivity of $F_{calc}(\mathbf{G})$ to the assumed Debye–Waller factors. Indeed the Debye–Waller factors available in literature for NiAl span a considerable range, i.e. for Ni 0.34 [31], 0.548 [32], 0.51 [30], 0.55 [33] and for Al 0.43 [31], 1.145 [32] and 0.47 [30], 0.44 [33]. This can create an uncertainty in $F_{calc}(\mathbf{G})$. For example, changing the values $B_{Ni} = 0.510$ and $B_{Al} = 0.470$ of Georgopoulos and Cohen [30] used here to the extreme literature [32] values of $B_{Al} = 1.145$ and $B_{Ni} = 0.548$ lowers our calculated $F_{calc}(200)$ from 22.99 to 21.74, i.e. even *below* the data of Fox and Tabbernor [9]. Although the values of Georgopoulos and Cohen [30] are the most accurate, this demonstrates the extreme sensitivity of $F_{calc}(\mathbf{G})$ to the values of B_α used.

In view of this possible uncertainty, it is interesting to treat the Debye–Waller factors B_{Ni} and B_{Al} (and their average) as adjustable parameters and least square fit our calculated $F_{calc}(\mathbf{G})$ of equation (9) to the measured $F_{expt}(\mathbf{G})$ values

$$\sum_{\mathbf{G}}^{(200)} \left| \left\{ \rho_I(\mathbf{G}) e^{-\langle B\rangle G^2/16\pi^2} + \sum_{\alpha=1}^{M} \rho_\alpha^{MT}(\mathbf{G}) e^{-B_\alpha G^2/16\pi^2} \right\} - F_{expt}(\mathbf{G}) \right|^2 = \text{Min.} \quad (19)$$

Table 1. Structure factors for NiAl (in units of e/cell), showing the results for the solid and for a superposition of atomic form factors, see text. The experimental data is from Fox and Tabbernor [9]. The superposition model $F_{sup}(\mathbf{G})$ is shown both for the local density approximation (LDA) and for Hartree–Fock (HF) taken from Table 1 of Fox and Tabbernor [9]

	Dynamic, solid		Dynamic, atoms		Static, solid	Static, atoms
hkl	$F_{calc}(\mathbf{G})$ [equation (9)]	$F_{expt}(\mathbf{G})$ [equation (1)]	$F_{sup}(\mathbf{G})$ LDA [equation (14)]	$F_{sup}(\mathbf{G})$ HF	$\rho_{calc}(\mathbf{G})$ [equation (7)]	$\rho_{sup}(\mathbf{G})$ [equation (13)]
100	13.45	13.53	13.23	13.28	13.67	13.44
110	28.07	28.08	28.12	28.25	28.91	28.97
111	10.23	10.30	10.22	10.32	10.74	10.73
200	22.99	22.60	23.00	23.12	24.40	24.42
210	8.27		8.31	8.34	8.97	9.01
211	19.50		19.48	19.55	21.32	21.31
220	16.83		16.82	16.86	18.96	18.96
300	6.06		6.10	6.06	7.02	7.06
221	6.07		6.10	6.06	7.03	7.06
310	14.72		14.74	14.75	17.10	17.11
311	5.39		5.42	5.38	6.45	6.48
222	13.06		13.07	13.07	15.62	15.63
320	4.88		4.90	4.86	6.03	6.05
321	11.70		11.71	11.70	14.42	14.44
400	10.57		10.59	10.57	13.43	13.45

Here, B_{Ni} and B_{Al} are adjustable parameters while ρ_I and ρ^{MT} are fixed by theory (Table 1). This yields rather reasonable values of $B_{Ni} = 0.56$ and $B_{Al} = 0.71$. The fitted values are

$$F_{fit}(100) = 13.47,\ F_{fit}(110) = 27.90,$$
$$F_{fit}(111) = 10.32,\ F_{fit}(200) = 22.71 \quad (20)$$

while the measured data are

$$F_{expt}(100) = 13.53,\ F_{expt}(110) = 28.08,$$
$$F_{expt}(11) = 10.30,\ F_{expt}(200) = 22.60. \quad (21)$$

The root mean square (rms) deviation is 0.11 e/cell while the rms deviation using B_α of Georgopoulos and Cohen [30] is 0.20 e/cell. This scatter in the Debye–Waller factors has only a minimal effect on our discussion below (Section 5.1) regarding the bonding properties of NiAl. This is so since in obtaining $F_{calc}(\mathbf{G})$ and $F_{sup}(\mathbf{G})$ [equation (19)], the Debye–Waller factors are applied both to $\rho_{calc}(\mathbf{G})$ [equation (9)] and to $\rho_{sup}(\mathbf{G})$. The change in B_α values will, however, drastically influence the discussion of Fox and Tabbernor since there the correction was applied only to find $F_{sup}(G)$. This point can be illustrated as follows: using our least square fitted Debye–Waller factors, we find that the dynamic superposition atomic structure factors (using Hartree–Fock data [17] as an example) are $F_{sup}(100) = 13.30$ and $F_{sup}(200) = 22.84$. Hence the different $|F_{expt}(\mathbf{G}) - F_{sup}(\mathbf{G})|$ for the "ionic" (100) component (0.23) and the "covalent" (200) component (0.24) are comparable. This is a rather different situation than what Fox and Tabbernor found: their difference for (200) was significantly larger (0.52) than the difference for (100) (0.25). This led them to conclude that the covalent (200) component of the DEDD overwhelms that of the ionic (100) piece.

The second possible source of error can be theoretical errors in calculating the *static* structure factors $\rho_{calc}(G)$. To test this we have examined the extent to which *ab initio* local density theory used here can reproduce experimental structure factors when the comparison is not clouded by uncertainties in the treatment of the temperature factors. We consider the *monoatomic* crystal Si. Here there is a single, symmetry-unique species α in the unit cell, so the temperature factor $T_\alpha(\mathbf{G}) = T(\mathbf{G})$ enters equations (1), (4) and (9) as a simple multiplicative factor of the *total* Fourier component $\rho(\mathbf{G})$. Table 2 compares the dynamic $F_{calc}(\mathbf{G})$, $F_{expt}(\mathbf{G})$ and static $\rho_{calc}(\mathbf{G})$ results for Si. $F_{expt}(\mathbf{G})$ is taken from Cummings and Hart [8]; this set represents the most

Table 2. Structure factors for Si in units e/cell. The difference δF_1 is $F_{calc}(\mathbf{G}) - F_{expt}(\mathbf{G})$ (in units of me/cell), while $\delta F_2 = F_{sup}(\mathbf{G}) - F_{expt}(\mathbf{G})$. The experimental data is from Cummings and Hart [8] except when otherwise noted. The Debye–Waller factor is $B = 0.4632$ (Ref. [36]). The root mean square deviation for δF_1 is 10 me/cell

	Dynamic, solid			Dynamic, atom		Static, solid	Static, atom
hkl	$F_{calc}(\mathbf{G})$ [equation (9)]	$F_{expt}(\mathbf{G})$ [equation (1)]	δF_1	$F_{sup}(\mathbf{G})$ [equation (14)]	δF_2	$\rho_{calc}(\mathbf{G})$ [equation (7)]	$\rho_{sup}(\mathbf{G})$ [equation (13)]
111	10.600	10.6025	−3	10.455	−148	10.726	10.579
220	8.397	8.3881	9	8.450	62	8.665	8.720
311	7.694	7.6814	13	7.814	133	8.033	8.159
222	0.161	0.1820[a]	−21	0.000	−182	0.168	0.000
400	6.998	6.9958	2	7.033	37	7.452	7.489
331	6.706	6.7264	−20	6.646	−80	7.225	7.161
422	6.094	6.1123	−18	6.077	−35	6.696	6.677
333	5.760	5.7806	−21	5.769	−12	6.404	6.415
511	5.781	5.7906	−10	5.769	−22	6.428	6.415
440	5.318	5.3324	−14	5.302	−30	6.030	6.012
531	5.054	5.0655[b]	−10	5.046	−20	5.799	5.790
442	0.008			0.000		0.009	0.000
620	4.662	4.6707[b]	−9	4.654	−17	5.455	5.446
533	4.451	4.4552[b]	−4	4.438	−17	5.269	5.255
444	4.115	4.1239	−9	4.107	−17	4.968	4.959
551	3.931	3.9349	−4	3.925	−10	4.802	4.795
711	3.929	3.9282[b]	1	3.925	−3	4.800	4.795
642	3.649	3.6558	−7	3.644	−12	4.546	4.541
553	3.494	3.5055[b]	−12	3.489	−17	4.404	4.399
731	3.493	3.4919[b]	1	3.489	−3	4.403	4.399
800	3.253	3.2485	5	3.251	3	4.182	4.179
733	3.122	3.1270[b]	−5	3.119	−8	4.062	4.057
660	2.917	2.9143	3	2.915	1	3.870	3.867
822	2.917	2.9111[b]	6	2.915	4	3.870	3.867
555	2.802	2.8009	1	2.802	1	3.761	3.761
751	2.804	2.8006[b]	3	2.802	1	3.764	3.761
840	2.628	2.6200[b]	8	2.627	7	3.598	3.596
753	2.529	2.5274[b]	2	2.529	2	3.503	3.504
911	2.530	2.5325[b]	−3	2.529	−4	3.505	3.504
664	2.380	2.3677[b]	12	2.378	10	3.362	3.360
844	2.165	2.1506	14	2.163	12	3.155	3.154
880	1.543	1.5325	11	1.542	10	2.551	2.549

[a]The "forbidden" (222) reflection is taken from Alkire *et al.* [34].
[b]Data from Saka and Kato [30] from which we subtracted the contributions of anomalous dispersion and nuclear scattering [8].

accurate measurements of crystalline structure factors to date. We also include in this table the "forbidden" (222) reflection measured by Alkire *et al.* [34] and the structure factors of Saka and Kato [35], from which we subtracted the contributions of anomalous dispersion and nuclear scattering [8]. The calculated values for Si were obtained in a precisely parallel way as those of NiAl, solving equation (18) using the LAPW method with the same numerical approximations. The Debye–Waller factor $B = 0.4632$ is used [36]. We see that theory reproduces experiment to within 20 me/cell for all measured reflections up to (880), i.e. 4–20 times better than in NiAl.

It hence appears that the larger discrepancies in NiAl (Table 1) could represent larger uncertainties in analyzing $F_{\text{expt}}(\mathbf{G})$ from the measurements. This point requires further investigation.

4.3. Sufficiency of low-angle structure factors to describe the overall deformation electron density distribution

We next examine whether the four lowest structure factors of NiAl (Table 1) amenable to high energy electron diffraction are sufficient to describe the main features of $\Delta\rho_{\text{sup}}(\mathbf{r})$. Since our calculation treats high and low **G** values equally, and since our results for low G are in reasonable accord with experiment, we examine this issue using in $\Delta\rho_{\text{sup}}(\mathbf{r})$ the *calculated* Fourier components $\rho_{\text{calc}}(\mathbf{G})$. Figure 4(a) shows the calculated static deformation density $\Delta\rho_{\text{sup}}(\mathbf{r}, G_{\max})$ of Table 1 including only $\mathbf{G} = (100)$, (110), (111) and (200) just as Fox and Tabbernor did, while Fig. 4(b) shows $\Delta\rho_{\text{rest}}$ contributed by the *remaining* **G** components, i.e. those above (200) [up to $2\pi/a(6, 3, 1)$]. Figure 4(c) then shows the sum of these contribution, i.e. the *total* calculated static deformation densities $\Delta\rho_{\text{sup}}(\mathbf{r}, G_{\text{big}})$. Solid lines represent positive $\Delta\rho$ values (charge accumulation relative to the superposition model), while dashed lines represent negative $\Delta\rho$ values. The thick solid lines next to a dashed line (label as "0") gives the $\Delta\rho = 0$ contour. We see that $\Delta\rho_{\text{rest}}(\mathbf{r})$ has qualitatively different features than the truncated $\Delta\rho_{\text{sup}}(\mathbf{r}, G_{\max})$. The former shows *accumulation* of charge on Al and "bonding" lobes near Ni pointing towards the Al site. Note that the magnitude of these effects is small near Al, so the truncated $\Delta\rho_{\text{sup}}(\mathbf{r}, G_{\max})$ [Fig. 4(a)] resembles closely the full $\Delta\rho_{\text{sup}}(\mathbf{r})$ of Fig. 4(c) in this region. However, the new features of $\Delta\rho_{\text{rest}}$ near Ni are large, so $\Delta\rho_{\text{sup}}(\mathbf{r}, G_{\max})$ of Fig. 4(a) misses them. A similar situation was found previously [11] in the covalently bonded GaAs crystal: limiting **G** to (111), (200), (400) and (333) reflections available to Zuo *et al.* [10] missed [11] significant features in $\Delta\rho_{\text{sup}}(\mathbf{r})$. Here too, truncation of the Fourier series for $\Delta\rho_{\text{sup}}$ in NiAl at $G_{\max} \leqslant (200)$ [Fig. 4(a)] misses completely the important directional covalent charge accumulation near Ni, shown in Fig. 3 as shaded areas.

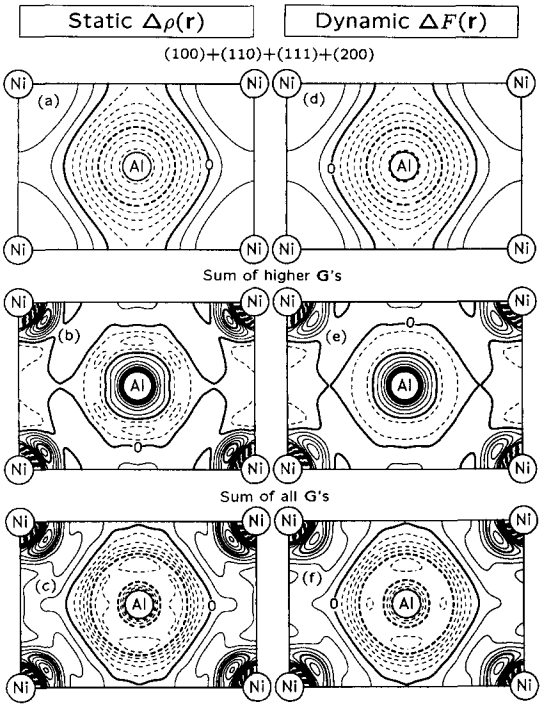

Fig. 4. Contour plots of the static and dynamic deformation density in the [110] plane of NiAl. Adjacent contours are separated by 0.01 e/Å^3; the zero contours are the thick solid contours labeled "0". (a) static $\Delta\rho$, including only (100), (110), (111) and (200). (b) static $\Delta\rho$ including terms above (200) up to $G_{\text{big}} = 2\pi/a(6, 3, 1)$. (c) static $\Delta\rho$ giving the sum of (a) + (b). Panels (c), (d) and (e) are the dynamic counterpart of (a), (b) and (c), respectively.

4.4. Static vs dynamic deformation electron density distributions

As discussed above, the immediate product of electron structure theory is the *static* density $\rho(\mathbf{r})$, while that of the diffraction experiment is the *dynamic* density $F(\mathbf{r})$; addition of temperature factors to the theory, or their deconvolution from experiment can be done only under some model assumptions. It is therefore of interest to compare the global features obtained in a *static* deformation density map $\Delta\rho_{\text{sup}}(\mathbf{r}, G_{\max})$ and a *dynamic* map $\Delta F_{\text{sup}}(\mathbf{r}, G_{\max})$. Considering the ratios $F_{\text{calc}}(\mathbf{G})/\rho_{\text{calc}}(\mathbf{G})$ and $F_{\text{sup}}(\mathbf{G})/\rho_{\text{sup}}(\mathbf{G})$ in Table 1, one notes only a very gradual attenuation of the structure factors due to the temperature effect: from 0.984 for $\mathbf{G} = (100)$ to 0.787 for $\mathbf{G} = (400)$. It is hence not obvious that in general, temperature effects will "wash out" the contribution of the high-Fourier components to $\Delta\rho_{\text{sup}}(\mathbf{r})$. To test this, we show in Fig. 4(d–f) the dynamic counterpart $\Delta F_{\text{sup}}(\mathbf{r}, G_{\max})$ to the static deformation map $\Delta\rho_{\text{sup}}(r, \mathbf{G}_{\max})$ shown in panels (a–c). We see that the static deformation map captures all features of the dynamic deformation map, in contrast with the expectation of Zuo *et al.* [20]. This means that (i) the current inability to measure accurately high-**G** structure factors poses a real limitation, as the $\Delta\rho(\mathbf{r})$ map is affected by these terms [compare Fig. 4(d) with

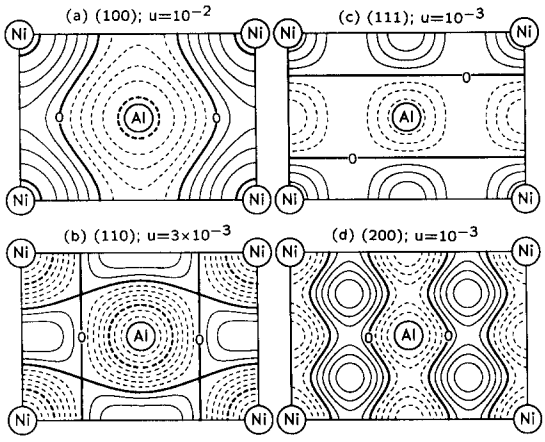

Fig. 5. Contour plots of the static deformation density in the [110] plane from individual Fourier component. The label "u" shows the units. (a) (100), units of 10^{-2} e/Å^3, (b) (110), units of 3×10^{-3} e/Å^3, (c) (111), units of 10^{-3} e/Å^3, and (d) (200), units of 10^{-3} e/Å^3. The (100) beam exhibits an "ionic" character, while (200) shows a "covalent" character. Note that the (100) component has the highest amplitude whereas (111) and (200) have the lowest.

Fig. 4(f)]. (ii) For many practical purposes it suffices to calculate the *static* map $\Delta\rho(\mathbf{r})$, as it captures most of the features of the dynamic map [compare Fig. 4(a) with 4(d) or 4(c) with 4(f)].

5. DISCUSSION OF THE GENERAL FEATURES OF BONDING CHARGE DENSITIES IN NiAl

5.1. Comparison with superposition of spherical neutral atoms

Figure 5 depicts the individual contributions of each of four lowest structure factors to the deformation electron distribution density in NiAl. As noted previously [9], the (100) and (111) structure factors contribute an "ionic" character, i.e. a depletion of charge from the Al region and a deposition of charge on the Ni region [and on the interstitial site for (111)]. In contrast, the (200) beam displays a "covalent" charge rearrangement highlighted in Fig. 5(d) by the directional accumulation of charge along chains *between* the Al and Ni sites. In the interstitial region (Figs 2 and 3), one notes the charge density is rather small and uniform exhibiting a metallic feature.

Note the scale of the various panels in Fig. 5: the calculated "ionic" contribution of the (100) beam has a considerably larger amplitude than the calculated "covalent" contribution of the (200) beam. Consequently, the total deformation density $\Delta\rho_{\text{sup}}$ or ΔF_{sup} [Fig. 4(a,c,d,f)] is dominated by the "ionic" piece. We conclude that NiAl exhibits both ionic and covalent (plus some metallic bonding components), but the "ionic" component dominates the total deformation densities measured with respect to a superposition of neutral atoms.

5.2. Comparison with the density of elemental solids

While the choice $\rho_{\text{model}}(\mathbf{r}) = \rho_{\text{sup}}(\mathbf{r})$ in equation (11) is the classic benchmark against which density deformation in the solid have been generally discussed, this choice is by no means unique. Much like the *cohesive* energy of a solid is taken with respect to the energy of the free atoms, while the *formation* energy is taken with respect to the energy of the solid elemental constituents, we can define a density redistribution with respect to the latter reference. Indeed, Fox and Tabbernor [9] found that $F_{\text{expt}}(\mathbf{G})$ of NiAl is closer to the values obtained from interpolation of the data on solid Ni and Al than it is to $F_{\text{sup}}(\mathbf{G})$.

Figure 6(a) shows as a line plot the difference between the self-consistently calculated charge density of NiAl and that of the elemental solids b.c.c.

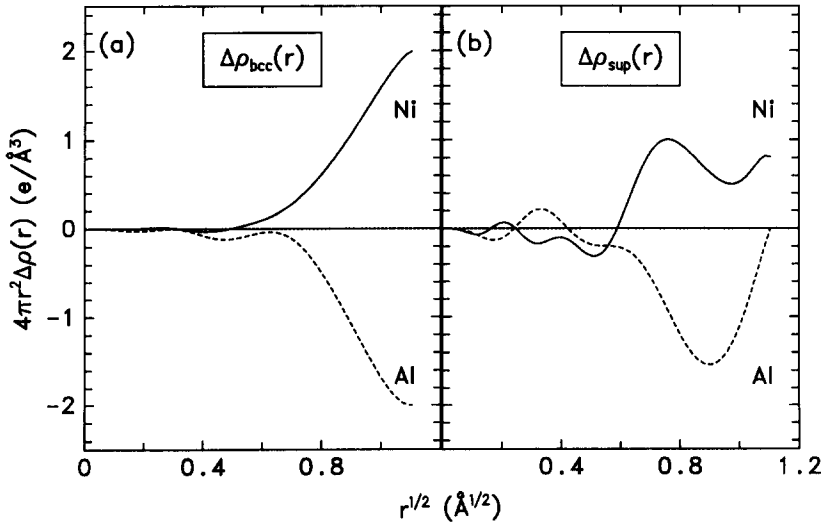

Fig. 6. The difference $\Delta\rho = \rho_{\text{calc}}(\mathbf{r}) - \rho_{\text{model}}(\mathbf{r})$ of equation (11) for two reference density: (a) ρ_{model} taken as the charge densities of b.c.c. Al or Ni at the molar volume of NiAl; (b) ρ_{model} taken as a superposition of ground state, spherical free atom densities.

Table 3. Angular decomposed charges inside muffin-tin spheres of radii $R_{MT} = 1.2171$ Å. The reference system is taken as elemental Ni and Al in the b.c.c. structure with the same molar volume as NiAl. Δ_{Ni} and Δ_{Al} show the difference $\int_0^{R_{MT}}[\rho_l(\text{NiAl}) - \rho_l(\alpha)]\,dr$ for α = Ni and Al. The charges outside R_{MT} make up the difference

	s	*p*	*d*	*f*	Total
Ni (CsCl)	0.435	0.438	8.397	0.010	9.281
Ni (b.c.c.)	0.409	0.345	8.259	0.021	9.040
Δ_{Ni}	0.026	0.093	0.138	−0.011	0.241
Al (CsCl)	0.617	0.763	0.173	0.025	1.584
Al (b.c.c.)	0.715	0.939	0.237	0.014	1.831
Δ_{Al}	−0.098	−0.176	−0.064	0.011	−0.247

Ni and Al at the same molar volume as NiAl. Table 3 shows a decomposition of this charge difference inside the muffin-tin spheres into angular momentum components. Figure 6(b) gives $\rho_{calc}(\mathbf{r}) - \rho_{sup}(\mathbf{r})$ for comparison with Fig. 6(a). These results show the following trends:

(i) Whether one uses as a reference density for $\rho_{model}(\mathbf{r})$ the solid state density of the constituents [Fig. 6(a)] or that of the superposed free atoms [Fig. 6(b)], Ni is seen to gain charge while Al loses charge.

(ii) Close to the muffin-tin sphere boundary, $\Delta\rho_{sup}$ is *smaller* than $\Delta\rho_{b.c.c.}$ indicating that an atomic reference model better describes there the crystalline charge density of NiAl. In contrast, closer to the atomic cores $\Delta\rho_{b.c.c.}$ is smaller than $\Delta\rho_{sup}$, indicating that a solid b.c.c. model better describes there the NiAl charge density.

(iii) While both reference models show that *overall*, Ni gains charge and Al loses charge, the $\Delta\rho_{sup}$ model shows that within 0.2 Å [0.45 $Å^{1/2}$ in Fig. 6(b)] from the origin, Ni *loses* charge while Al *gains* charge.

(iv) Inspection of the *orbital* character of the charge rearrangement relative to the solid elements (Table 3), shows that Ni in NiAl *gains* ~ 0.03, 0.10 and 0.14 electrons in the *s*, *p* and *d* shells, respectively, while Al in NiAl *loses* −0.10, −0.18 and −0.06 e in these respective shells. Hence, the main bonding effects are loss of Al *sp* charge (−0.27 e) and gain of Ni *pd* charge (0.23 e).

6. SUMMARY

Our main findings can be summarized as follows (see list of questions articulated in the Introduction):

1. If one uses the Debye–Waller factors used by Fox and Tabbernor, *ab initio* band theory describes the lowest three measured dynamic factors of NiAl with an accuracy of 80 me/cell while the calculated (200) term is ~ 400 me/cell higher than the value deduced from experiment. The scatter in the Debye–Waller factors leads to a higher uncertainty [> 1000 me/cell in $F(200)$]. We tentatively attribute the differences between theory and experiment to imperfections in the data analysis, i.e. to the way that temperature factors are associated with individual scattering contributions from sites [$\rho_\alpha(\mathbf{G})$ with $T_\alpha(\mathbf{G})$ in equation (1)]. Treating the Debye–Waller factors as adjustable parameters yields $B_{Ni} = 0.56$ and $B_{Al} = 0.71$ (compare with $B_{Ni} = 0.51$ and $B_{Al} = 0.47$ believed to be the most accurate for NiAl used by Fox and Tabbernor). This reduces the error of the fitted theory vs experiment to 110 me/cell. The difference between experiment and theory regarding the (200) structure factor exists and awaits further study. In the case of a monoatomic crystal such as Si, where $T_\alpha(\mathbf{G})$ is α-independent, the agreement between theory and experiment is excellent: to within ~ 20 me/cell up to $\mathbf{G} = (880)$; see Table 2.

2. Exclusion of the high index structure factors $\mathbf{G} > (200)$ from the Fourier series of $\Delta\rho_{sup}$ does not significantly alter the qualitative picture of deformation electron density distribution near Al. In contrast, important covalent features are missed by this truncated DEDD near the Ni sites. This is similar to the situation in the covalently bonded GaAs [11], where omission of $F(\mathbf{G})$ for $\mathbf{G} = (311)$, and (222) significantly changed the DEDD.

3. The overall shape of the deformation electron density is similar in a static $\Delta\rho_{sup}(\mathbf{r})$ and dynamic $\Delta F_{sup}(\mathbf{r})$ maps, so either can be used to assess the DEDD.

4. NiAl exhibit both "ionic" [(100) and (111)] and "covalent" [(200)] plus "metallic" contributions to bonding. The ionic piece is dominant in the total deformation electron density distribution.

5. Comparing the crystalline density to the models of (a) superposition of neutral, spherical ground state atoms, and (b) solid elemental Ni and Al, we find that both exhibit gain of charge by Ni and loss by Al.

Acknowledgements—Useful discussion and comments on the manuscript by Professor A. G. Fox are gratefully acknowledged. This work was supported by the Office of Energy Research (OER) [Division of Materials Science of the Office of Basic Science (BES)], U.S. Department of Energy, under contract No. DE-AC02-77-CH00178.

REFERENCES

1. P. J. E. Aldred and M. Hart, *Proc. R. Soc. A* **332,** 223 (1973).
2. T. Takama and S. Sato, *Phil. Mag.* **B45,** 615 (1982).
3. A. G. Fox and R. M. Fisher, *Phil. Mag.* **B57,** 197 (1988); *Aust. J. Phys.* **41,** 461 (1988).
4. M. A. Tabbernor and A. G. Fox, *Phil. Mag. Lett.* **62,** 291 (1990).
5. J. R. Schneider, N. K. Hansen and H. Kretschmer, *Acta crystallogr.* **A37,** 711 (1981).
6. N. K. Hansen, J. R. Schneider and F. K. Larsen, *Phys. Rev.* **B29,** 917 (1984).
7. F. K. Larsen and N. K. Hansen, *Acta crystallogr.* **B40,** 169 (1984).
8. S. Cummings and M. Hart, *Aust. J. Phys.* **41,** 423 (1988).
9. A. G. Fox and M. A. Tabbernor, *Acta metall. mater.* **39,** 669 (1991).
10. J. M. Zuo, J. C. H. Spence and M. O'Keeffe, *Phys. Rev. Lett.* **61,** 353 (1988).
11. J. E. Bernard and A. Zunger, *Phys. Rev. Lett.* **62,** 2328 (1989).
12. P. Hohenberg and W. Kohn, *Phys. Rev.* **136,** B864.
13. W. Kohn and L. J. Sham, *Phys. Rev.* **140,** A1133 (1965).

14. B. Dawson, *Proc. R. Soc. A* **298,** 264 (1967); *ibid* **298,** 379 (1967).
15. M. Deutsch, *Phys. Lett. A* **153,** 368 (1991).
16. J. E. Jaffe and A. Zunger, *Phys. Rev. B* **28,** 5822 (1983).
17. P. A. Doyle and P. S. Turner, *Acta crystallogr.* **A24,** 390 (1968).
18. F. Herman and S. Skillman, *Atomic Structure Calculations.* Prentice-Hall, Englewood Cliff, N.J. (1963).
19. Z. W. Lu, S.-H. Wei and A. Zunger, *Phys. Rev. B* **44,** 3387 (1991).
20. J. M. Zuo, J. C. Spence and M. O'Keeffe, *Phys. Rev. Lett.* **62,** 2329 (1989).
21. D. Hackenbracht and J. Kübler, *J. Phys. F* **10,** 427 (1980).
22. (a) T. Hong and A. J. Freeman, *Phys. Rev. B* **43,** 6446 (1991); (b) C. L. Fu and M. H. Yoo, *Acta metall. mater.* **40,** 703 (1992).
23. K. J. Kim, B. N. Harmon and D. W. Lynch, *Phys. Rev. B* **43,** 1948 (1991).
24. S.-C. Lui, J. W. Davenport, E. W. Plummer, D. W. Zehner and G. W. Fernando, *Phys. Rev. B* **42,** 1582 (1990).
25. Z. W. Lu, S.-H. Wei, A. Zunger, S. Frota-Pessoa and L. G. Ferreira, *Phys. Rev. B* **44,** 512 (1991).
26. D. M. Ceperley and B. J. Alder, *Phys. Rev. Lett.* **45,** 566 (1980).
27. J. P. Perdew and A. Zunger, *Phys. Rev. B* **23,** 5048 (1981).
28. S.-H. Wei and H. Krakauer, *Phys. Rev. Lett.* **55,** 1200 (1985), and references cited therein.
29. P. Villars and L. Calvert, *Pearson's Handbook of Crystallographic Data for Intermetallic Phases.* Am. Soc. Metals, Metals Park, Ohio (1985).
30. P. Georgopoulos and J. B. Cohen, *Scripta metall.* **11,** 147 (1977).
31. M. J. Cooper, *Phil. Mag.* **8,** 811 (1963).
32. T. Hughes, E. P. Lautenschlager, J. B. Cohen and J. O. Brittain, *J. appl. Phys.* **42,** 3705 (1971).
33. M. Mosteller, R. M. Nicklow, D. M. Zehner, S.-C. Lui, J. M. Mundena and E. W. Plummer, *Phys. Rev. B* **40,** 2856 (1989).
34. R. W. Alkire, W. B. Yelon and J. R. Schneider, *Phys. Rev. B* **26,** 3097 (1982).
35. T. Saka and N. Kato, *Acta crystallogr.* **A42,** 469 (1986).
36. M. Deutsch, M. Hart and P. Sommer-Larsen, *Phys. Rev. B* **40,** 11666 (1989).